Dolomite in archaeological plaster: An FTIR study of the plaster floors at Neolithic Motza, Israel

Yonah Maor, Michael Toffolo, Yishay Feldman, Jacob Vardi, Hamoudi Khalaily, Yotam Asscher

Dolomite in archaeological plaster:

An FTIR study of the plaster floors at Neolithic Motza, Israel

Yonah Maor[1]*, Michael B. Toffolo[2,3], Yishay Feldman[4], Jacob Vardi[1], Hamoudi Khalaily[1], Yotam Asscher[1]

[1] Israel Antiquities Authority, P.O. box 586, Jerusalem, 9100402, Israel

[2] Archéosciences Bordeaux, UMR 6034 CNRS, Université Bordeaux Montaigne, 8 Esplanade des Antilles, 33607 Pessac, France

[3] Geochronology and Geology Program, Centro Nacional de Investigación sobre la Evolución Humana (CENIEH), Paseo Sierra de Atapuerca 3, 09002 Burgos, Spain

[4] Department of Chemical Research Support, Weizmann Institute of Science, Rehovot 7610001 Israel

*Corresponding author

Abstract

Material studies of ancient plaster can provide invaluable information on pyro-technological advancements, living practices, stylistic preferences and possibly the cultural organization needed to produce the plaster. Past studies have established methods of analysis for calcite and gypsum-based plaster, but studies of dolomite-rich plaster can be more complicated. In particular, the useful FTIR-based method for determining the structural organization of calcite, which differentiates pyrogenic and geological calcite, is hindered by the overlapping calcite and dolomite peaks. Therefore, a new FTIR-based calibration is presented for quantifying the dolomite percent of the carbonates. This was tested both on known mixtures and in comparison to XRD analyses of ancient plaster. Weighted mixtures of calcite and dolomite were used to demonstrate the problem that dolomite causes when using FTIR to study calcite's structural order. Limits were established for when dolomite can be considered a small error versus when additional steps must be taken, such as a density separation step to separate disordered calcite from dolomite-rich samples. These methods were applied to a case study of red-painted plaster floors from PPNB Motza. Two types of plaster were found: the plaster preparation layers which contained large aggregates and, based on the new calibration, a high percent of dolomite and some soil, while the finishing topcoat was almost pure calcite with finer aggregates. The same technology persisted across the examined PPNB building phases. Additional examination by light microscopy was able to clarify the outlier results and provide possible insight on the use of a sunken floor or basin. These methods can now be applied for comparison studies of plaster across sites and time periods, and could also be useful in geological studies where mixtures of calcite and dolomite are present.

1. Introduction

Plaster production is one of the earliest pyrotechnological achievements documented in the southern Levant. The production of plaster was well-known during the Pre-Pottery Neolithic period (9,400-6,600 B.C cal.) in early stages of the agricultural revolution while the earliest

examples of plaster use were already documented in the late Natufian (12,800-10,800 B.C cal), and in the Final Natufian (10,800-9,800 B.C cal.) as well (Friesem et al., 2019; Gourdin & Kingery, 1975; Grosman et al., 2020; Kingery et al., 1988). Plaster made in these periods in the Mediterranean climatic regions was mainly for the fabrication of plastered floors; however, in some cases, walls and various installations were also coated with plaster. The extent of the phenomenon of plastered floors is so widespread to the point that almost every Pre-Pottery Neolithic B (hereafter PPNB) village across the Levant included plaster-paved dwelling units or public buildings, for example: Yiftahel, Beisamoun, Kfar Hahoresh (Goren & Goring-Morris, 2008; Khalaily et al., 2008; LeChevallier, 1978; Poduska et al., 2012).

Analytical examination of ancient plaster has advanced archaeological studies in various aspects: plaster as a significant development of ancient technology (Goren & Goldberg, 1991), as a testimony to the living practices of the Neolithic societies (Garfinkel, 1987), the stylistic preferences at the time (Anderson et al., 2014; Schirmer, 1990), and the cultural organization of Neolithic communities (Kingery et al., 1988).

Various analytical methods have been used in such plaster studies, with X-ray diffraction, scanning electron microscopy and light-microscopy in particular providing useful structural, chemical and mineralogical information (Diekamp et al., 2009; Goren & Goring-Morris, 2008; Karkanas, 2007; Miriello et al., 2011; Regev, Zukerman, et al., 2010; Thuesen et al., 1990). In the past decade, a Fourier transform infrared (FTIR) spectroscopy method, known as grinding curves, has become increasingly common in lime-plaster research (Asscher et al., 2020; Poduska et al., 2011; Regev, Poduska, et al., 2010; Toffolo et al., 2019, 2020; Xu et al., 2015). This method can quickly determine if calcite is pyrogenic plaster or geological in origin and indicates the state of preservation of plaster. Thus, many samples can be analyzed for a better comparison of building trends or practices. Unfortunately, this method cannot be used when dolomite is a significant component, as the calcite and dolomite peaks overlap in the FTIR spectrum.

Lime plaster is typically created by burning limestone in a kiln or a pit to temperatures in the range of 800-900 ^{o}C for a period of time between hours to days (Boynton, 1980). The main mineral in limestone, calcite ($CaCO_3$), undergoes calcination when burned above 700 ^{o}C. Carbon dioxide is released, leaving behind quicklime (CaO). Lime is slaked by mixing with water, which results in calcium hydroxide, $Ca(OH)_2$. This soft malleable paste can be spread or shaped into any desired form. Often aggregates such as sand, crushed stones or sediment are added to the plaster. The aggregates serve to both expand the volume of the lime plaster and improve its mechanical properties upon drying (Artioli, 2010). During the setting of the paste, a reaction takes place between atmospheric CO_2 and the calcium hydroxide to form calcite again. The newly formed calcite crystals show different structural and morphological properties compared to the original materials (Regev, Poduska, et al., 2010; Toffolo et al., 2020).

This altered calcite structure is utilized in the FTIR grinding curve method, a rapid method to characterize lime plaster based on the interpretation of the ratios of the CO_3 group vibrational bands in the calcitic fraction of the binder. Three of the infrared absorption peaks in transmission mode correspond to the asymmetric stretch (1420 cm^{-1}), out of-plane bending (874 cm^{-1}) and in-plane bending (713 cm^{-1}) vibrations of the CO_3 group, commonly referred to ν_3, ν_2, and ν_4, respectively (Farmer, 1974). The normalized heights of these absorption

bands are correlated with the degree of atomic disorder in calcite, allowing to differentiate between calcites of different origins such as geological and pyrogenic materials (Chu et al., 2008). This is because the ν_4 in calcite is strongly affected by heating (Xu & Poduska, 2014) and other causes of disorder (Xu et al., 2016) commonly found in pyrogenic plaster (Poduska et al., 2012). The ν_4 becomes broader and its intensity decreases relative to the ν_2 and ν_3, which are less affected. Particle-size related optical scattering of the infrared light influences peak heights and their interpretation; therefore, a method for decoupling scattering from true absorption was developed, in which the KBr pellet necessary for transmission mode is measured multiple times at different levels of grinding and particle size distribution. The resulting plots show well-separated trend lines for different types of calcite (Poduska et al., 2011; Regev, Poduska, et al., 2010).

Dolomite, $CaMg(CO_3)_2$, has a very similar structure to calcite and consequently also has a very similar FTIR spectrum, with absorption peaks shifted from those of calcite due to the magnesium ions incorporated in the lattice. The dolomite ν_4 peak is at 728 cm^{-1} and therefore fully separated from the calcite peak at 713 cm^{-1}. On the other hand, the ν_2 peak at 881 cm^{-1} overlaps with the calcite ν_2 peak at 875 cm^{-1}. This means that if we were to use the grinding curve method in its original format, by comparing the height of the absorbance peaks at 713 and 875 cm^{-1}, we would in fact be comparing an inflated value for the ν_2 peak due to the dolomite contribution. A similar phenomenon was observed when aragonite was mixed with calcite, influencing the interpretation of the grinding curves of lime binders that contain aragonite (Toffolo et al., 2019). In addition to being found as an aggregate in plaster, dolomite can also be burnt to make plaster, though the reaction pathways are more complex with many possible products forming (Al-Bashaireh, 2008; Bruni et al., 1997; Caroselli et al., 2020; Newton & Sharp, 1987).

In this work, dolomite and calcite mixtures were quantified based on FTIR spectra and the method was validated by comparing to XRD analysis. The quantification was then used to estimate the influence of dolomite on peak-ratio analysis of calcite. Accordingly, the limitations of the grinding curve method in identifying well-preserved lime binders that contain dolomite can now be explored. Finally, these methods were used to compare and categorize dolomite-rich Neolithic plaster floors from the recent excavations at Motza wherein several settlements attributed to the PPNB included dozens of plastered floors and installations. Demonstrating how large numbers of floors could be quickly surveyed and grouped by their mineralogical composition and assessing differences between building phases and types of plastered surfaces.

1.1 The Motza excavation:

The case study presented in this paper is based on the examination of plaster floors of a single structure recently uncovered during a large salvage excavation project conducted at Motza (ca. five kilometers west of Jerusalem, by the modern-day village of Motza 'Illit, Judea Mt. Israel). The site was investigated several times in the past. The part known as Tell Motza was examined in the early 90's and later during 2003 (Greenhut et al., 2009), uncovering settlements from the Ottoman, Iron age and Bronze age settlements. Within the lowest four

meters of that excavation, the remains of middle PPNB (hereafter MPPNB) and early PPNB (EPPNB) settlement were uncovered. Two structures are worth noting: one with a square-shaped room and another that had a rounded construction. Both structures' floors were plastered.

Prior to the development of the area and the construction of a new highway entrance to Jerusalem, a large area was excavated between 2015 and 2021 covering over three hectares by the Arza stream (a tributary channel of the Soreq stream). The excavation uncovered a huge Pre-Pottery Neolithic settlement with the largest and most extensive building phase relating to the final PPNB period (which can be roughly dated to 7,100-6,700 B.C. cal.). The remains of an earlier settlement, dating from the MPPNB, were uncovered as well, mostly under extensive FPPNB site remains or under other later chronological phases. The excavations by the Arza stream on the eastern slope of Mt. Motza uncovered settlement remains of other periods starting at the middle Epipaleolithic until the Late 19th century (Ad & Eirikh-rose, 2021; Khalaily & Vardi, 2019; Vardi & Khalaily, 2021). The excavation uncovered over a hundred plaster floors, some exceptionally well-preserved and coated with red paint attributed to the MPPNB and to the FPPNB (Khalaily & Vardi, 2020; Vardi & Khalaily, 2021). It seems that the later plaster floors, from the FPPNB onwards, are different in texture. They are thinner in comparison to the plaster floors of the MPPNB and are crumblier and more porous.

1.2 Building B10 case study:

Materials for this study were from the largest structure found at the site (Figure 1). It is a rectangular building, in sub-area B10, which was divided into four rooms with a total area covering 150 m^2. Three separate construction phases were identified, all of which were ascribed to the MPPNB period, with phase I being the lowest and phase III the highest. Besides the plaster floors, the building contains several pits, some plastered, a hearth, and burials under floors. One feature of interest is an approximately elliptical basin (L.4681) in phase I. This could be considered an additional lower floor, or it could be an installation with some other function. It was included in this study to be compared to clearly defined floors. The larger floors, especially L.4622, the floor of the main room in building phase II, were clearly created by several separate plaster applications in sections as distinct borders between some of these plaster sections have been preserved. In total, 28 samples (Table 1) were taken from approximately 10 separate plaster applications that made six floor/surface features in these three construction phases. Some floors were sampled in multiple locations for reproducibility. A section of the large floor in L.4666 (Figure 1 - phase I) was dismantled, allowing the use of a well-preserved Neolithic plaster in experiments simulating mixtures of calcitic plaster and dolomite.

Figure 1: Mid-late PPNB structure from area B10 in Motza with many plaster floors. The three building phase top plans (marked I-III) include the sampling locations. Aerial field photo (©Assaf Peretz): North is marked with a red arrow and a white arrow points to the sunken basin L.4681. Each square was 5X5 m.

Table 1: Plaster surface samples used in the area B10 case-study. Loci and sample numbers are as marked on the plans in Figure 1. Basket numbers are the original sample numbers provided by the excavators.

Sample #	building phase	Locus	basket	Description of samples
1	Phase I	4666	135550	Prep layer only
2			136129	
3			136330	
4			136323	Prep layer with red painted topcoat (paint partially preserved)
5			136322	

6			136135	
7			136429	
8*			136421	
9**			136421	Red painted topcoat only.
10		4681	136136	Prep layer with red painted "topcoat" (brown topcoat, rather than white)
11			136321	
12		4721	136134	Prep layer only
13	Phase II	4622	136132	Prep layer only
14			135740	
15			22/7/18-#8	
16			136130	
17			136329	Prep layer and topcoat
18			136126	Prep layer only
19			136326	Prep layer and topcoat
20			136426	Topcoat only
21			136125	Prep layer only
22			136325	
23			136332	Prep layer and topcoat
24			136131	Prep layer only
25			136427	Red painted topcoat only
26		4716	136124	Prep layer and red painted topcoat
27			136127	Prep layer and thick (~5 mm) topcoat
28	Phase II/III	4642	136122	Prep layer and thick (~5 mm) topcoat

*Sample 8 is large plaster chunks from dismantling a section of floor L.4666; many sub-samples of Sample 8 were examined.

**Sample 9 is apparently the lower stage of floor L.4666 uncovered during the dismantling.

2. Materials and Methods:

2.1 Reference materials:

Homogenized mixtures of standard samples were prepared: large calcite spar crystal (Ward's catalog no. 49H1600) and Motza bedrock (pure dolomite by FTIR analysis, see Figure 2b). The calcite crystal and dolomite stone were thoroughly crushed and homogenized by mortar and pestle. Samples of each were weighed and mixed at ratios 9:1, 3:1, 1:1, 1:3 and 1:9. For the plaster reference, the unpainted topcoat on an area of several centimeters of floor L.4666 (Sample 8) was separated, crushed, and homogenized. This topcoat was almost pure calcite (see XRD analysis, Figure 3c) and was very fine-grained. According to the grinding curve method, this topcoat was almost as disordered as modern plaster. This Neolithic plaster was then mixed in with weighted amounts of dolomite to simulate mixtures of calcite plaster and dolomite aggregate.

2.2 Methods

FTIR (Fourier Transform Infra-Red): The Nicolet iS5 model with iD1 attachment was used for transmission measurements on KBr pellets. For small features in archaeological specimens, samples were taken from clean areas with a scalpel knife, crushed by mortar and pestle and mixed with KBr. The mixture of KBr and sample was pressed in a PIKE hand-press and measured once a clear pellet formed. Results, averaged from 32 scans at 4 cm^{-1} resolution in the 400-4000 cm^{-1} range, were compared to a database of standards. For standards and bulk archaeological specimens, a similar method was used, except several grams were crushed and homogenized before taking small sub-samples and adding KBr. In this way, both the binder and aggregates were examined. Peak heights and ratios were measured relative to the baseline using a macro written for this purpose in Omnic Macro Basic software. The macro finds local minima in the ranges around each peak, excluding areas where other common components in plaster may cause interference, and draws a baseline between them (Table 2).

Table 2: Peak positions and baselines of vibrational bands used to calculate peaks heights, and atomic disorder based on peak ratios. For each peak the baseline is defined by two points selected at the local minimum in the spectral region here indicated. Peak heights were normalized relative to the main ν_3 carbonate peak.

Vibrational mode	Peak position (cm^{-1})	Baseline (cm^{-1})
ν_3 (CO_3) calcite & dolomite	1400-1480 (local maxima in range)	2330–1450/1450–715
ν_2 (CO_3) calcite	875	950–875/875–795
ν_4 (CO_3) calcite	713	775–713/660–615
ν_4 (CO_3) dolomite	728	775–713/660–615

XRD (X-ray Diffraction): Powder diffraction measurements were carried out in reflection geometry using a TTRAX III (Rigaku, Japan) diffractometer equipped with a rotating Cu anode operating at 50 kV and 200 mA and with a scintillation detector aligned at the diffracted beam after a bent Graphite monochromator. $2\theta/\theta$ scans were performed at specular conditions in Bragg-Brentano mode with variable slits and scanned from 20 to 90 degrees of 2θ with a step size of 0.025 degrees and scan speed of 2 degrees per minute. Quantitative phase analysis was performed using the PDF-4 + 2020 database (ICDD) and Jade Pro software (Materials Data, Inc.) by Whole Pattern Fitting module (Pawley method).

Light microscopy: Select samples of plaster floors were cut with a diamond saw and polished to expose a cross-section of the plaster. Friable samples were first embedded in epoxy or polyester resin before cutting. Zeiss Stereo Discovery V12 microscope with a 5 megapixel Axiocam 105 color camera was used for photographing thick sections at magnifications of X8-X100. For thin sections, embedded samples were glued to microscope slides, cut, ground down and polished to 30 µm thickness. These were examined under plain polarized light

(PPL) and cross-polarized light (XPL) at magnifications of X25-X500 with the Zeiss Axioscope 5 microscope attached to the Axiocam 105 color camera.

Density separation: Archaeological plaster samples were powdered using an agate mortar and pestle and prepared following the method of Toffolo et al. (2020) in order to separate calcite from dolomite based on their different densities, which are 2.71 and 2.86 g/cm³, respectively. Toffolo et al. (2020) showed that pyrogenic calcite exhibits lower density compared to its geogenic counterpart, with values around 2.5 g/cm^3, which makes it easier to separate the dolomite by centrifugation in a heavy liquid. This difference in density is presumably caused by structural defects in the pyrogenic form that result in less tightly packed carbonate groups. Therefore, sodium polytungstate (SPT) was set accordingly at density ρ=2.65 g/cm³ (including buffer).

3. Results & Discussion:

To assess the amount of dolomite in plaster samples, homogenized mixtures of standard samples were prepared. Figure 2 shows the calibration curve based on mixtures of calcite spar and dolomite, using the peak heights of the ν_4 peaks at 713 cm^{-1} for calcite and 728 cm^{-1} for dolomite (data in Table SI-1). We used the ratio of dolomite to the total carbonates rather than a simple dolomite to calcite ratio to avoid emphasizing variation in small peaks due to instrumental noise. The linear fit with the intercept set to zero (R^2=0.99), shows that FTIR can accurately estimate the percentage of dolomite in a mixture, even when done in field conditions. Since the calcite ν_4 peak height is affected by disorder in plaster as well as the amount, using this calibration for plaster could introduce a degree of error. To estimate the error, we compared the calcite spar crystal mixtures to a very well-preserved sample of Neolithic plaster (L.4666), which is disordered calcite with a low ν_4 peak. This plaster was mixed with weighted amounts of dolomite, and the FTIR analysis of the resulting peak heights are shown alongside the calibration curve, indicating up to 15% error (Figure 2b).

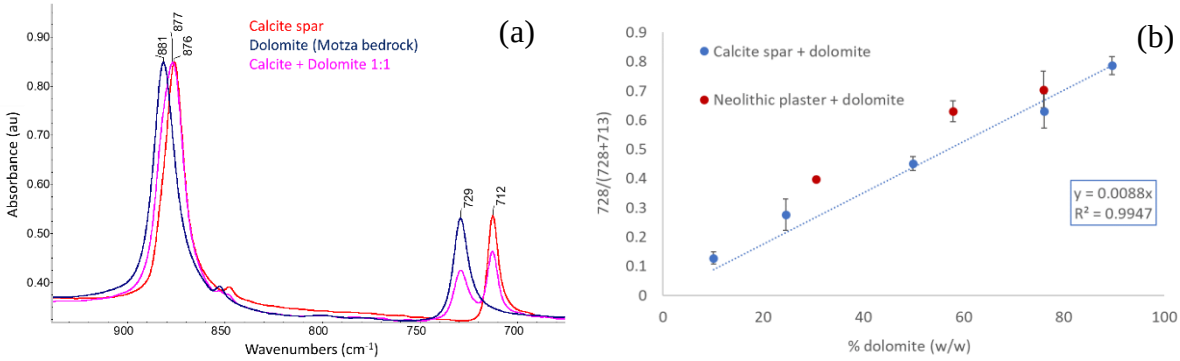

Figure 2: (a) FTIR spectra of calcite spar, dolomite from the Motza bedrock, and a 1:1 mixture of the two. (b) Calibration curve quantifying % dolomite of the total carbonates based on known mixtures of calcite spar and dolomite (Motza bedrock) and known mixtures of Neolithic calcite plaster with dolomite added for comparison (n=9).

The calibration presented here was validated by the well-established XRD quantification. Samples of Motza plaster with varying amounts of dolomite (by FTIR) were tested by XRD

and representative diffractograms are shown in Figure 3. The full quantification of calcite and dolomite is included in Table 3. A strong correlation is found between the FTIR and XRD assessment of the dolomite content (Figure 4), corroborating the FTIR method, even for ancient plaster.

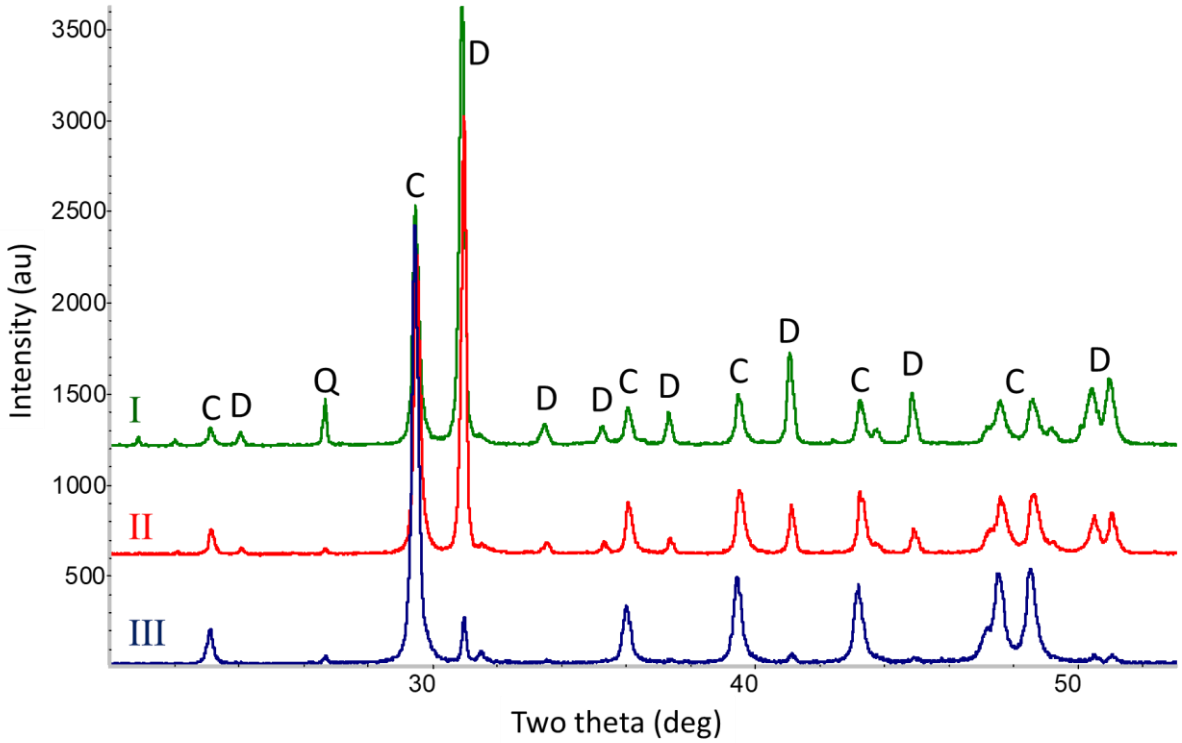

Figure 3: Representative XRD diffractograms of samples with varying amounts of dolomite. I) Prep layer B.135552, II) Installation inner coat B.136328, III) Topcoat B.136421. Peak assignments are labeled: C=Calcite, D=Dolomite and Q=Quartz.

Table 3: XRD quantification of samples with varying amounts (weight %) of calcite and dolomite (small amounts of additional minerals, such as quartz or mica not shown).

Description	Locus	Basket	XRD	
			% calcite	% dolomite
Plaster floor - prep layer	4544	136336	42.2	53.6
Plaster floor - prep layer	4544	135552	35.2	61.2
Plastered installation - prep layer	4635	136328	49.1	49.2
Plastered installation - inner coat	4635	136328	59.0	40.4
Plaster floor - prep layer	4666	136322	57.0	42.6
Plaster floor - topcoat	4666	136429	90.4	8.0
Plaster floor - topcoat	4666	136421	92.8	6.3
Plaster floor - topcoat	4622	136426	95.4	4.1
Plaster floor - topcoat	4635	136427	86.4	8.7
Plaster floor - topcoat	4666	136428	92.9	6.0

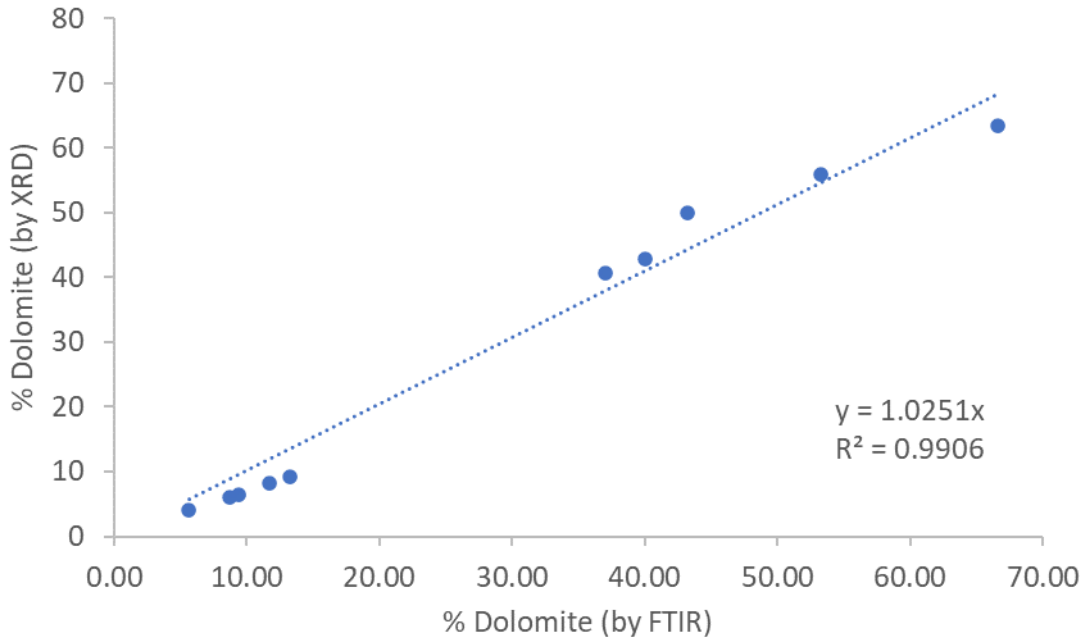

Figure 4: Comparison of % dolomite of total carbonates quantified by FTIR calibration and by XRD.

The calcite spar and dolomite mixtures were also used to determine the influence of dolomite on the reliability of plaster characterization using the calcite grinding curves. In high dolomite content, the ν_2 peak of dolomite at 881 cm^{-1} will cause the absorbance at the calcite ν_2 (875 cm^{-1}) to be larger than it would be if calcite only were present, leading to misinterpretation of the atomic disorder. This effect is illustrated in Figure 5a. As the ratio of dolomite to calcite increases the ν_4 values become smaller as there is less calcite, but the relative ν_2 values remain high as it represents both calcite and dolomite. Samples with small amounts of dolomite (ex. ratio 9:1) show minute shifts and the interpretation of the atomic disorder is unchanged; however, when large amounts of dolomite are present this very ordered geological spar could even be mistaken for plaster. The ν_3 peak used to normalize the spectra is also a combination of calcite and dolomite; however, in this case it is only used to account for variation in sample size, and the materials have similar extinction coefficients (Lane, 1999; Querry, 1987), so the total peak height does not introduce a significant error.

It may seem that up to a 1:1 mixture the error is still not enough to confuse geological and pyrogenic calcite. It is important to keep in mind that when testing an unknown sample, the local calcite stone may be as disordered as chalk (blue line in Figure 5). Presumably, even low levels of dolomite mixed with chalk, or recrystallized plaster, could cause the data to fall near the modern plaster reference (green line in Figure 5). For this reason, caution is needed when using the grinding curve methods as soon as any amount of dolomite is observed. The calcite found around Motza is more ordered limestone and not chalk (see below); therefore, the grinding curve method could be reliable with up to 30% dolomite.

The examination of the effect of dolomite on the grinding curves is completed by checking the mixtures of well-preserved, disordered Neolithic plaster with dolomite. Figure 5b shows that the trend continues; samples move from the plaster line towards the most disordered reference – ash burned at 900 °C (light blue line in Figure 5b) when dolomite is added. This

means that if a sample containing both calcite and dolomite falls high enough on the grinding curves (above the modern plaster reference), we can assume it is pyrogenic plaster despite the error caused by dolomite.

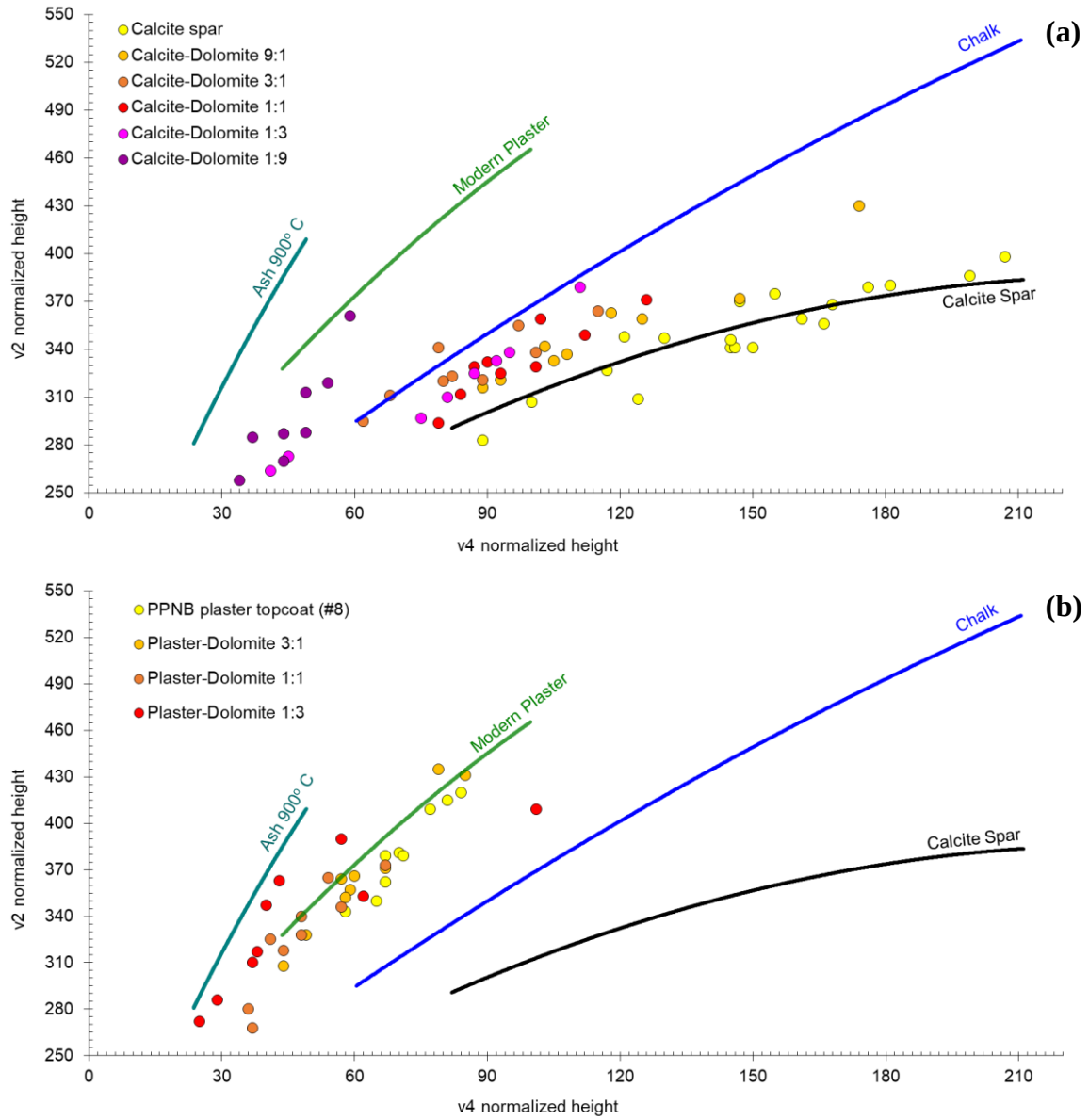

Figure 5: Grinding curve plot with references to a range of calcite samples recreated from Regev et al (2010). Adding the normalized ν_2 and ν_4 peak heights for (a) Calcite spar with gradually greater ratio of dolomite mixed in. (b) Neolithic plaster with gradually greater ratio of dolomite mixed in.

Case study of middle PPNB plaster floors in area B10 in Motza:

Visual observations of a typical well-preserved Neolithic plaster floor at Motza shows the following structure: a lower foundation layer of stones and sediment, a middle preparation layer of plaster (henceforth 'prep layer') that ranges between 1-10 cm thick with many aggregates, and a smooth white topcoat, usually 1-2 mm thick. The topcoat was coated with a

thin layer of red paint. Although some floors did not have the red paint or even the topcoat, it is difficult to say if they were never there or if it is a difference in preservation. This structure of prep layer and topcoat is very similar to that found at the PPNB sites of Yiftahel (Poduska et al., 2012) and 'Ain Ghazal (Rollefson, 1990). The aggregates in the prep layer range in size from microns to several millimeters across. The binder in the prep layer is often light hued, varying from off-white, light brown, light pink, and yellow tints. The boundary between the foundation and the prep layer was not always clearly defined, suggesting wet plaster had infiltrated the foundation. The topcoat appeared fine-grained and uniform when observed in the field; however, under magnification aggregates were clearly visible in all topcoats.

Photomicrographs of plaster cross sections clearly show the aggregates in both layers (Figure 6). For the most part, topcoat aggregates are white and relatively small, under 1 mm, so they blend in with the white binder, implying that aggregates were crushed and sifted during topcoat preparation. In some cases, for example floor L.4617 seen in Figure 6b, there are occasional brown aggregates and a long (2-3 mm) white aggregate. Evidence of maintenance is observed in L.4666, where a browner plaster covered a white typical topcoat (Figure 6a). The white layer sloped off, probably worn down by use, and the plaster was leveled using a beige plaster, which was then repainted red. A closer look at this reapplied topcoat, Figure 6c, shows it is still lighter in color than the prep layer below it. The red paint layer was measured on five samples and was found to vary between 20-150 µm in thickness. The general floor structure is summarized by the diagram in Figure 6d. Additional details are seen in petrographic thin sections, for example Figure 6e shows the different matrixes of crust (encrusted sediment over the paint), paint, topcoat and prep layer in "basin" L.4681. Figure 6f shows the three mineral aggregates found in these floors, calcite, dolomite and quartz, where the first two are by far the more common aggregates. The iron-rich red paint layer includes hematite and goethite; the full analysis of the paint will be published in a subsequent paper.

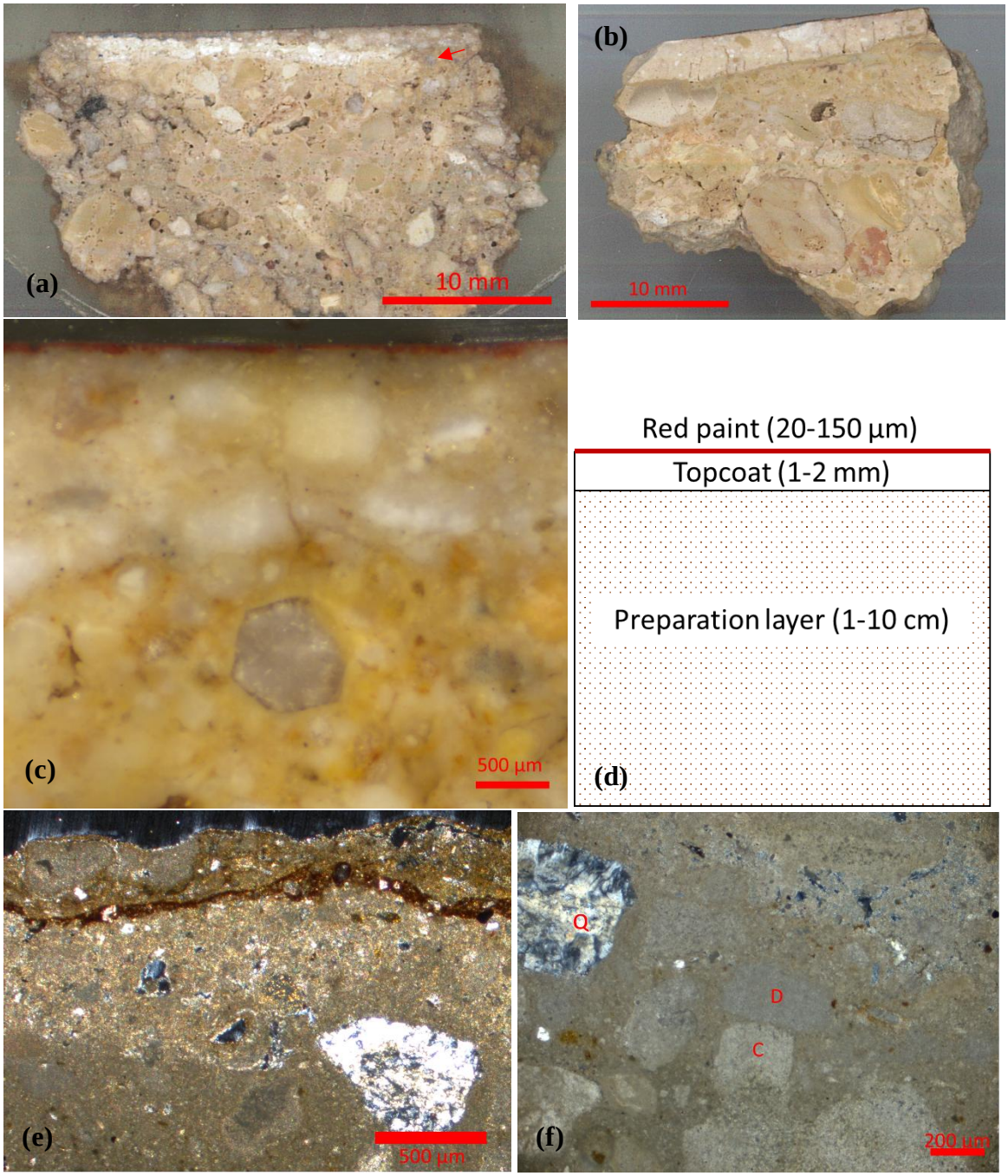

Figure 6: Structure of plaster floors in area B10. (a) Cross section from main floor (L. 4666, #6) with two types of topcoat. Arrow marks hexagonal quartz crystal seen in micrograph c. (b) Cross section with uniform topcoat (L. 4617, #26). (c) Stereoscope image of paint, topcoat, and prep-layer in main floor (L.4666, #6). (d) Diagram of typical floor structure. (e) XPL image of crust, paint, topcoat, and prep layer in "basin" (L.4681, #10) (f) XPL of typical aggregates Q-quartz, D-dolomite, C-calcite (L.4681, #10).

Plaster samples from area B10 were characterized by FTIR, evaluating the composition of the topcoat (if present) and its associated prep layer. These were bulk measurements, including both binder and aggregates. A representative IR spectrum of a prep layer shows mainly

calcite, dolomite, some clay, and minor amounts of quartz (Figure 7a). The clay and quartz main peaks overlap to form a peak in the range 1030-1084 cm^{-1}, as both contain Si-O bonds. The exact position varies by the mixture present and if the clay has been fired or not (Berna et al., 2007). This peak is marked Si and used to represent all the silicate minerals. The combined calcite and dolomite ν_3 peak (at 1436 cm^{-1} in the example below) is labeled CO_3 and is used to represent all the carbonates. The ratio of these two peak heights Si/CO_3 is a useful indication of the amount of sediment (clay and quartz) mixed into the plaster. The percent dolomite out of the total carbonates (calcite and dolomite) is calculated from the ν_4 peaks, marked C and D in the spectrum, according to the calibration method described above.

A plot of the Si/CO_3 and % dolomite of the two plaster layers across the three different building phases (architectural plans in Figure 1) shows a clear difference in the compositions of the topcoat and the prep layer (Figure 7b, Table SI-2). In general, the topcoats were close to pure calcite, with no more than 20% dolomite and with a low Si/CO_3 ratio (under 0.15) indicating that very little sediment is present. In contrast, the prep layer mostly varies between 30-60% dolomite and has a higher Si/CO_3 ratio (above 0.15). This trend holds across all the building phases, indicating a consistent technology, not only in the basic structure of the plaster floors, but also in the materials chosen to prepare the different layers (in Figure 7b phase 1 is marked with squares, phase 2 in circles, phase 3 in diamonds).

Ancient Motza is situated on the Soreq formation, so the bedrock directly under the site is dominated by dolomite and marly dolomites, with negligible amounts of marly calcites (Arkin & Ecker, 2007; Roskin et al., 2022). The Soreq stream and its tributary, which runs just by the site bring a mixture of calcite and dolomite pebbles. Nowadays, there are exposures further upstream which are the direct source of the calcite. Due to modern construction and erosion, it is not possible to know how far the Neolithic occupants of Motza would have been required to travel to find a similar calcite exposure.

The builders clearly chose to use large quantities of the readily available dolomitic bedrock in the prep layer and saved the calcitic rocks for the finishing topcoat. There is also a clear preference for adding crushed carbonates as aggregates rather than sediment, which creates a stronger plaster (Scannell et al., 2014). However, they were only careful to exclude all sediment in the topcoat. The dolomite aggregates in particular can improve water resistance of the plaster (Štukovnik et al., 2020). It is possible the PPNB builders knew about these advantageous mechanical properties and so went to the trouble of crushing stones rather than mixing in sediment as was done at many other sites

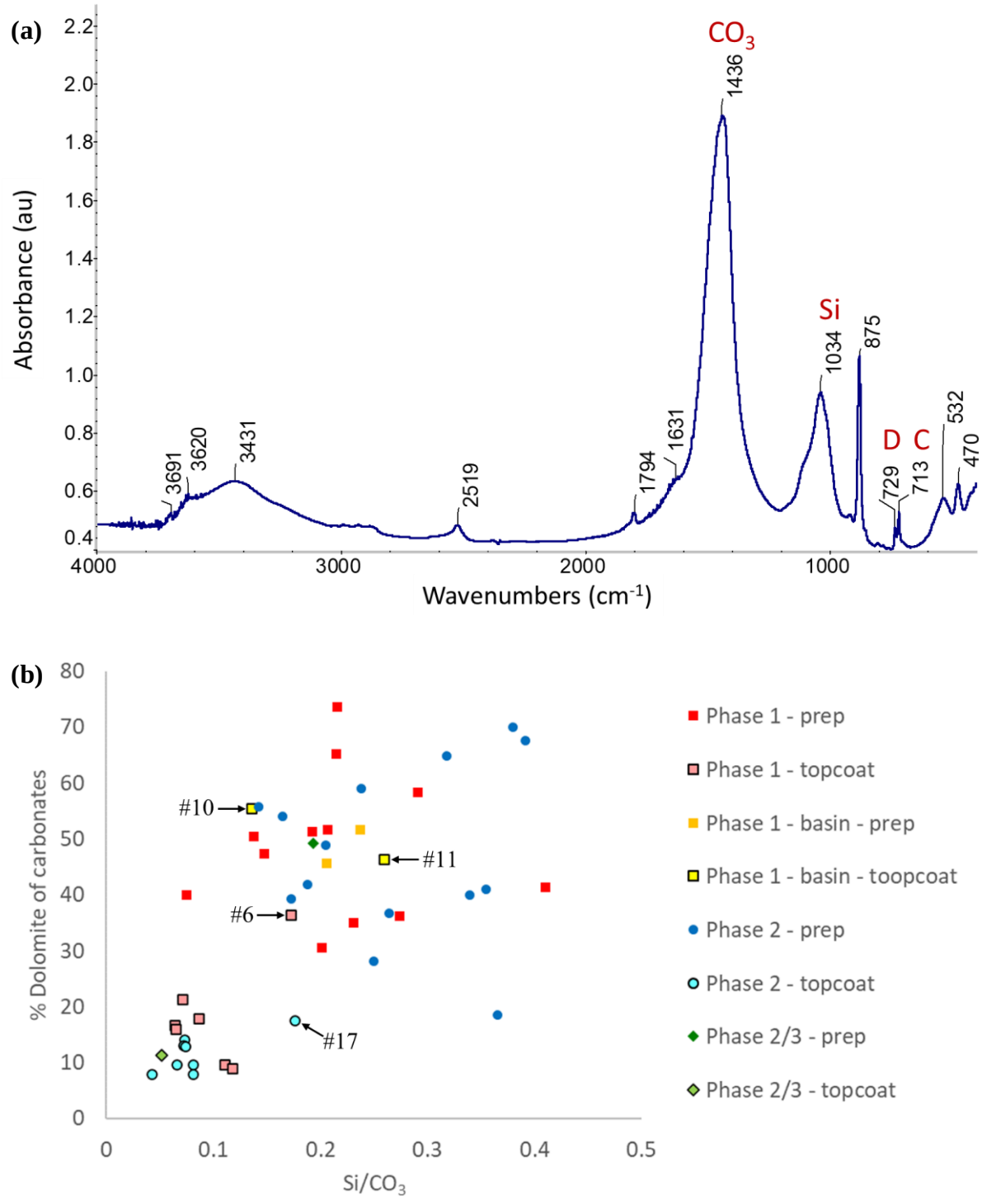

Figure 7: (a) Typical FTIR spectrum of bulk plaster preparation layer with peaks used in calculations marked. Si=silicates, CO_3=carbonates, C=calcite, D=dolomite. (b) Distribution of plaster samples by comparing the ratio of silicates to carbonates and the % dolomite of carbonates. Squares are phase 1, circles are phase 2 and diamonds for phase 2/3. Darker colors represent the prep layer and lighter color with frames are the topcoat. Arrows and sample-numbers mark outliers.

There are a few exceptions to the trend described above. Two topcoat floor measurements (samples 6 and 17) have a Si/CO_3 ratio of 0.17-0.18, somewhat higher than typical (marked with arrows in Figure 7b). In topcoat #17 this slightly higher sediment level is due to the crust on top of the plaster, which was included in the measurement, unlike in the other samples. In topcoat #6 on the other hand, there is also higher than normal dolomite (36%). This was examined further via its cross section (Figure 6a and c), which showed that the white topcoat was re-plastered with a beige topcoat, as discussed above. The darker color in the re-plastered layer is explained by the additional sediment and dolomite in the plaster. We hypothesize that the PPNB residents of Motza preferred using pure calcite for the finishing topcoat, but it was harder to obtain, so when a quick fix was required to the damaged floor, they chose to compromise with a mixture including more dolomite.

In addition, Samples 10 and 11 from surface L.4681, which is the plastered basin or sunken floor in floor L.4666 (marked with a white arrow in Figure 1), also show interesting results. The topcoat samples all fall in the range of the dolomite-rich prep layers, suggesting a different construction technique. This is also supported by examination of a cross section of the "basin" surface (Figure 8), which shows that while there is a distinct ~1 mm layer just under the paint, it is not the typical white topcoat. This observation was noted in different areas of the basin; therefore, it is unlikely to be a case of a localized repair as seen in Sample 6 from L.4666 (above). The "topcoat" of L.4681 appears even darker than its prep layer binder (Figure 8a). However, examination under magnification (Figure 8b) suggests that this may be an illusion caused by the aggregates in the prep layer. Instead, the binders in both layers are in fact very similar in appearance. This corresponds to their similar composition, with high silicates and dolomite content, as seen in the FTIR results. The only real difference is that the "topcoat" has much smaller aggregates than the prep layer, like all the plaster floors examined, and that the topcoat may be less dense, as seen in XPL images (Figure 6 e, f). The red-painted surface eliminates the possibility that a pure calcitic topcoat was initially present but eroded. We can speculate that the dolomite-rich topcoat was deliberately applied. If the basin was used to retain liquids, dolomite-rich plaster might have been chosen for improved water resistance (Štukovnik et al., 2020); nonetheless, we cannot exclude that there was a lack of available calcite when this feature was plastered.

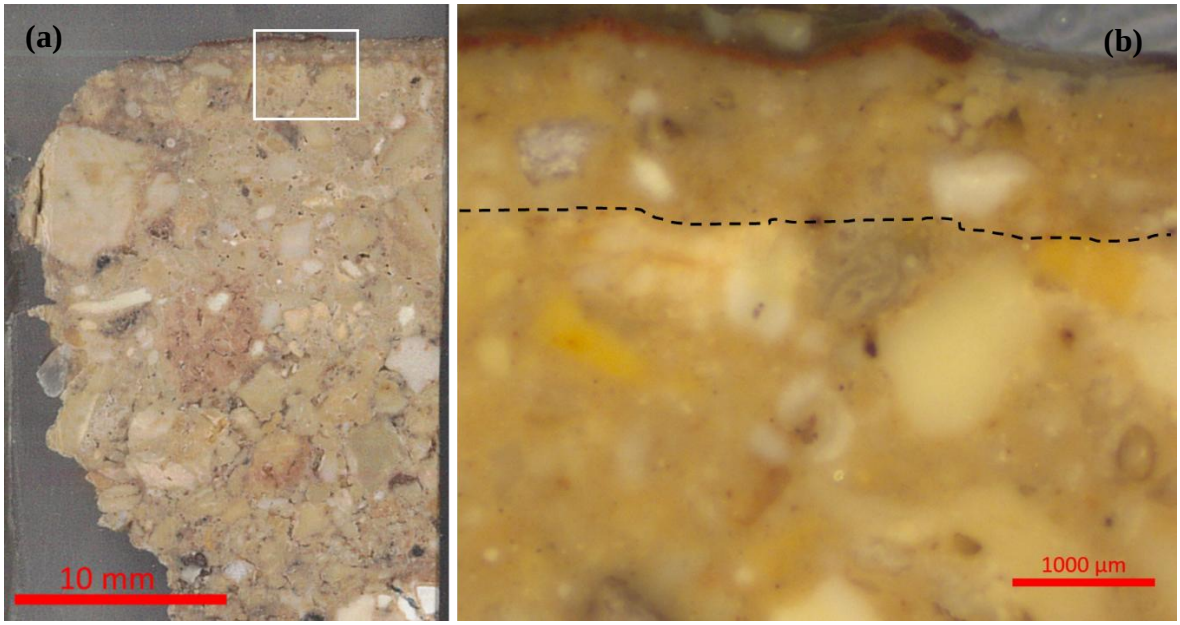

Figure 8: Cross section of surface 4681 (the "basin"). (a) Scan of the section. Box marks the area shown at higher magnification. (b) Stereoscope image of crust, red paint, "topcoat" and prep-layer. Dashed line marks the interface between the layers.

The level of calcite disorder can also be used to compare plaster floors – whether they are well-preserved pyrogenic plaster, recrystallized plaster or contain many limestone aggregates. Motza is situated in the Judean hills where the geological calcite is limestone and not chalk (Roskin et al., 2022); therefore, it was presumed that the grinding curves with the established calcite references may be reliable even up to 30% dolomite. To verify this, calcite stones from the nearby Soreq stream were analyzed for their level of calcite disorder (Figure 9), confirming that they all fall below the chalk line on the grinding curves. With that limit established, all the topcoat samples except "basin" L.4681 have low enough percentages of dolomite and therefore could be analyzed for their atomic disorder. All these samples fell on or near the modern plaster line, showing an incredible level of preservation for Neolithic plaster and further confirming the similarity of their construction technology regardless of the building phase. Two samples, however, showed low disorder relative to the modern plaster reference, both from floor L.4716. That floor's cross section (Figure 6b) shows a few larger aggregates, which may be more ordered limestone (this topcoat contains only ~1% dolomite), which could explain the higher order in the calcite topcoat of that floor.

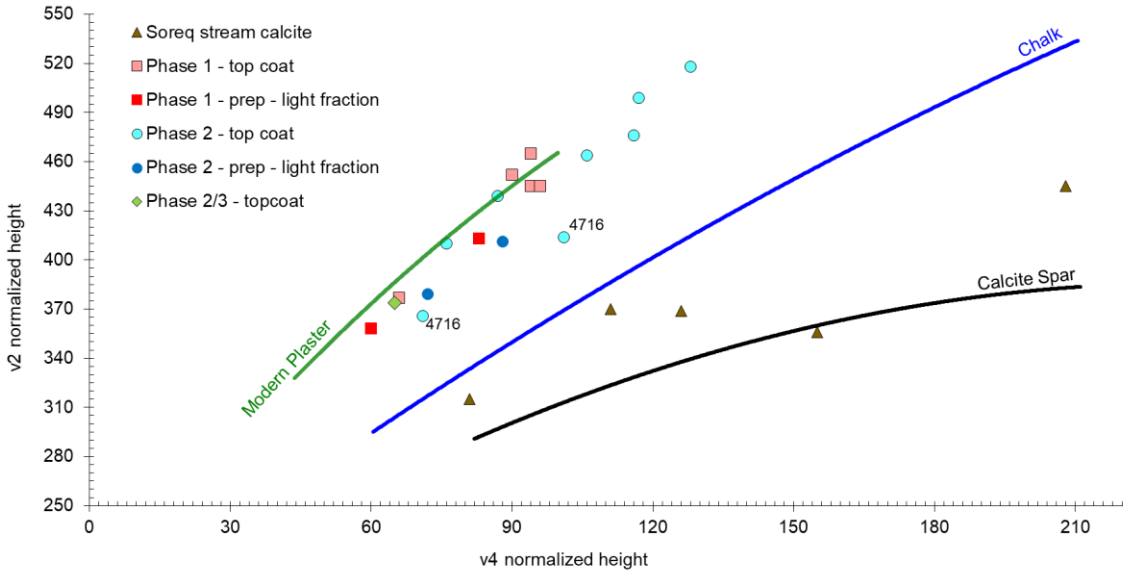

Figure 9: Grinding curve plot with references to a range of calcite samples recreated from Regev et al (2010). Showing normalized ν_2 and ν_4 peak heights of calcite stones from the Soreq stream, Neolithic plaster samples from the different building phases – topcoat samples used as is and prep layer samples after SPT separation to remove dolomite.

This project established constraints for using the grinding curve method in studying dolomite-rich plaster. In the case of Motza, as shown, the limit was established at 30% dolomite, which meant many preparation layer samples were excluded. To assess the atomic disorder of the binder in samples where dolomite content is above 30%, a different approach was taken, based on density separation since dolomite (2.86 g/cm³) is heavier than pyrogenic calcite (~2.5 g/cm³). The light fraction of plaster samples treated with SPT (see methods section for details) showed a marked decrease in the intensity of the dolomite ν_4 compared to the relative heavy fraction (Figure 10). The grinding curve method may thus be applied to determine the degree of atomic order of calcite crystals in the light fraction. This information may also be used in the selection of suitable samples for radiocarbon dating (Toffolo et al. 2020). For the Motza case study, two prep layer samples from each of the main building phases were separated and the calcite-rich light fractions were added to the grinding curve plot (Figure 9). The results confirm that the prep layer also contains pyrogenic calcite plaster. The two building phases show very similar level of disorder, further supporting the continuity of PPNB construction methods at the site.

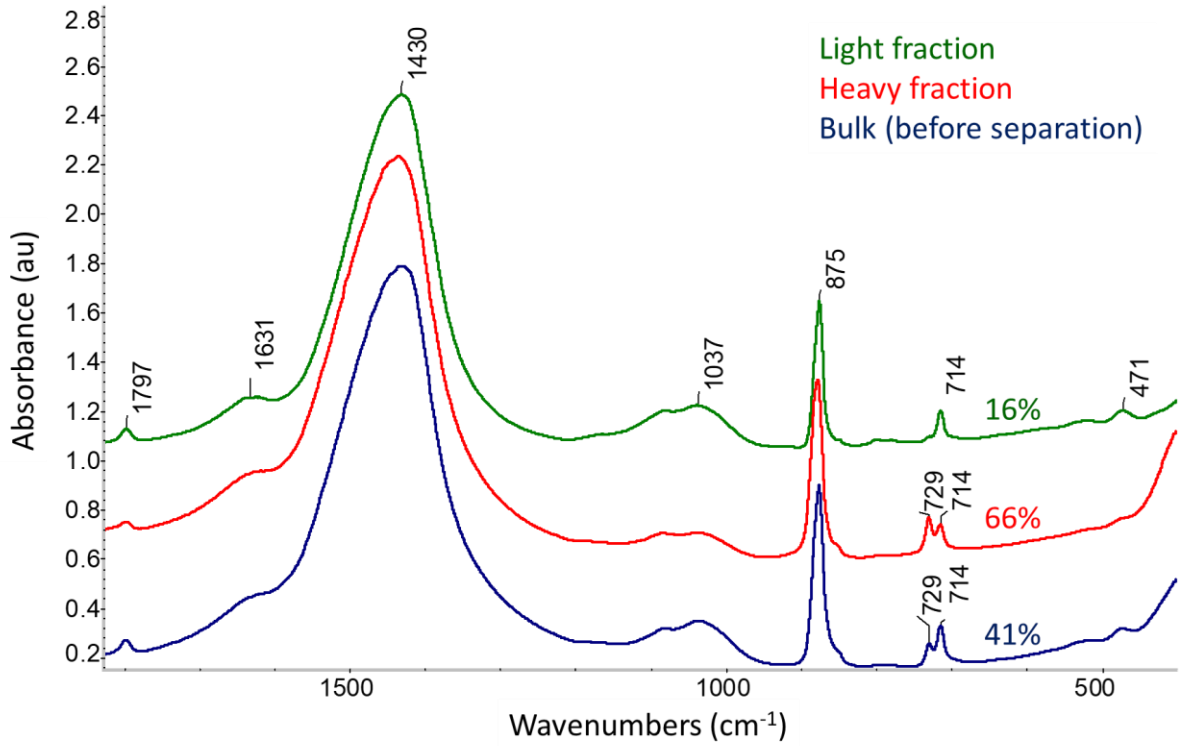

Figure 10: FTIR spectra of the prep layer in sample #5 before and after density separation by SPT, with the % dolomite of total carbonates marked by the ν_4 peaks (714 - calcite, 729 - dolomite). Blue – bulk before separation, Red – heavy fraction after separation, Green – Light fraction after separation. Spectra offset for clarity.

Overall, the new FTIR method applied to the case study of the plaster floors in the Motza B10 structure produced interesting results. The mineralogical analysis using the percent dolomite and the silicate to carbonate layer showed two distinct methods of plaster preparation. The local dolomite was used extensively in the prep layer and pure calcite was preferred for the finishing topcoat. This could be related to the brighter white color of the calcite plaster. The artisans would have had to work harder to find and bring in calcite. These two stones can be virtually identical in appearance and their ability to differentiate them is surprising and impressive. The level of calcite disorder showed that all binders were pyrogenic plaster, in other words, made from stones fired above 700 °C for complete decarbonization, and are well-preserved to this day. This high level of technology was consistent across the building phases found in this PPNB structure.

The combination of FTIR, with a new analysis adapted to dolomite, and light microscopy can now be applied further. A future report will show these methods used to compare plaster floors across the entire Motza excavation, comparing the plaster technologies in different types of PPNB structures or in different areas of the large excavation. Then additional comparisons can be made to the plaster technologies of later settlement periods at Motza, including the Bronze Age, Roman and Byzantine periods (Ad & Eirikh-rose, 2021). It will be enlightening to see how the different cultures adapted the use of the same local materials over time. Furthermore, these methods now allow easy comparison of the Motza results to other sites where plaster was studied by FTIR. Thus, the similar structure of the Motza floors to

Yiftahel's PPNB plaster floors can now be expanded to include a similar choice of carbonate aggregates, wherein sorting of small aggregates was only for the topcoat and both sites have well-preserved disordered plaster in the topcoats. The main difference between the sites is the use of the local dolomite in Motza prep-layers, while Yiftahel used only calcite (Poduska et al., 2012). Expanding to other types of plaster and other analytical methods, the plastered skull from Kfar Hahoresh was studied by inductively coupled plasma (ICP) and was found to have a filler plaster with a high percent of Si and an outer plaster forming the face with a much lower Si content (Hershkovitz et al., 1995), which is analogous to the prep and topcoat system in the Motza floors. Additional comparative studies could be done with any PPNB sites with plaster finds.

Dolomite is a widely occurring sedimentary rock and is common all over the world (Boggs, 1995; Warren, 2000), therefore the FTIR method presented here could have applications beyond the obvious archaeology or historic conservation. In recent years, there has been great interest in using dolomite in various forms as a more environmentally friendly option than standard cement (Agrawal et al., 2021; Jeon et al., 2021; Zhang et al., 2021). In geological research, open questions still exist about the formation of dolomite and the conversion of calcite to dolomite, known as 'the dolomite problem' (Chang et al., 2020; Ryb & Eiler, 2018). Mapping dolomite locations is also important because significant proportions of the world's gas, oil and other hydrocarbons are found in dolomite reservoirs. Dolomite is also important in the mineralization of many useful ores (Warren, 2000). All these types of studies and others may find use for this FTIR characterization method, both for quantifying the dolomite in mixed calcite-dolomite rocks and as an additional approach to assess the type/order of the calcite.

4. Conclusions:

The FTIR-based method presented here facilitates study of dolomite-rich plaster and allows differentiation of plaster types by their minerology. Using the quantification of dolomite, a method for assessing the calcite disorder despite the presence of dolomite has been presented, with limits for when the 'grinding curve' method can be used and when an additional separation step is necessary. For Motza, the limit was set at 30% dolomite of the total carbonates, based on the local calcite which is ordered limestone and not chalk. This adaptation of the 'grinding curves' is useful both for comparing plaster technology or preservation and for finding samples suitable for Carbon-14 dating. In the application of these methods to the Motza case study, two plaster types were found, one for the prep layer and another for the topcoats. These two methods were used consistently across the PPNB building phases. This approach can now be used to compare plaster across other archaeological sites and time periods.

5. Acknowledgments:

The Israel Antiquities Authority salvage excavations at Motza, headed by Jacob Vardi and Hamoudi Khalaily (licenses A-8248 and A-8411) and the subsequent research were funded by the National Transport Infrastructure Company of Israel (Netivei Israel). Michael Toffolo was supported by a grant from IdEx Bordeaux (grant n. ANR-10-IDEX-03-02). The authors

thank B10 area manager, Ayelet Segal for her interest and help collecting samples, Dmitry Yegorov for many discussions on plaster making at Motza, Doa'a Salman for the B10 top-plans, Assaf Peretz for field photography and Ilana Peters for her assistance with editing the manuscript.

6. References:

Ad, U., & Eirikh-Rose, A. (2021). Moza , Highway 1 - Preliminary Report. *Hadashot Arkheologiyot*, *133*.

Agrawal, Y., Gupta, T., Siddique, S., & Sharma, R. K. (2021). Potential of dolomite industrial waste as construction material: a review. *Innovative Infrastructure Solutions*, *6*(4), 1–15. https://doi.org/10.1007/s41062-021-00570-5

Al-Bashaireh, K. S. (2008). *Chronology and Technological Production Styles of Nabatean and Roman Plasters and Mortars at Petra (Jordan)*. The University of Arizona.

Anderson, E., Almond, M. J., Matthews, W., Cinque, G., & Frogley, M. D. (2014). Analysis of Red Pigments from the Neolithic sites of Çatalhö yük in Turkey and Sheikh-e Abad in Iran. *Spectrochimica Acta - Part A: Molecular and Biomolecular Spectroscopy*, *131*, 373–383. https://doi.org/10.1016/j.saa.2014.03.126

Arkin, Y., & Ecker, A. (2007). *Geotechnical and Hydrogeological Concerns in Developing the Infrastructure Around Jerusalem*. Geological Survey of Israel.

Artioli, G. (2010). *Scientific Methods and Cultural Heritage: An introduction to the application of materials science to archaeometry and conservation science*. Oxford University Press.

Asscher, Y., Van Zuiden, A., Elimelech, C., Gendelman, P., Ad, U., Sharvit, J., Secco, M., Ricci, G., & Artioli, G. (2020). Prescreening Hydraulic Lime-Binders for Disordered Calcite in Caesarea Maritima: Characterizing the Chemical Environment Using FTIR. *Radiocarbon*, *62*(3), 527–543. https://doi.org/10.1017/RDC.2020.20

Berna, F., Behar, A., Shahack-Gross, R., Berg, J., Boaretto, E., Gilboa, A., Sharon, I., Shalev, S., Shilstein, S., Yahalom-Mack, N., Zorn, J. R., & Weiner, S. (2007). Sediments exposed to high temperatures: reconstructing pyrotechnological processes in Late Bronze and Iron Age Strata at Tel Dor (Israel). *Journal of Archaeological Science*, *34*(3), 358–373. https://doi.org/10.1016/j.jas.2006.05.011

Boggs, S. (1995). *Principles of Sedimentology and Stratigraphy*. Prentice Hall.

Boynton, R. S. (1980). *Chemistry and Technology of Lime and Limestone, 2nd Edition*. Wiley.

Bruni, S., Cariati, F., Fermo, P., Cairati, P., Alessandrini, G., & Toniolo, L. (1997). White lumps in fifth- to seventeenth-century AD mortars from Northern Italy. *Archaeometry*, *39*(1), 1–7. https://doi.org/10.1111/j.1475-4754.1997.tb00786.x

Caroselli, M., Hajdas, I., & Cassitti, P. (2020). Radiocarbon dating of dolomitic mortars from the Convent Saint John, Mustair (Switzerland): first results. *Radiocarbon*, *62*(3), 601–615. https://doi.org/10.1017/RDC.2020.35

Chang, B., Chang, B., Li, C., Liu, D., Foster, I., Tripati, A., Tripati, A., Tripati, A., Lloyd, M. K., Maradiaga, I., Maradiaga, I., Luo, G., An, Z., She, Z., Xie, S., Tong, J., Huang, J., Algeo, T. J., Algeo, T. J., … Immenhauser, A. (2020). Massive formation of early diagenetic dolomite in the Ediacaran ocean: Constraints on the "dolomite problem." *Proceedings of the National Academy of Sciences of the United States of America*, *117*(25). https://doi.org/10.1073/pnas.1916673117

Chu, V., Regev, L., Weiner, S., & Boaretto, E. (2008). Differentiating between anthropogenic calcite in plaster, ash and natural calcite using infrared spectroscopy: implications in archaeology. *Journal of Archaeological Science*, *35*(4), 905–911. https://doi.org/10.1016/j.jas.2007.06.024

Diekamp, A., Konzett, J., Mirwald, P. W., & Tyrol, S. (2009). Magnesian lime mortars - identification of magnesium-phases in medieval mortars and plasters with imaging techniques. *12th Euroseminar on Microscopy Applied to Building Materials*, *September*, 309–318.

Farmer, V. C. (1974). *Infrared spectra of minerals*. Mineralogical Society.

Friesem, D. E., Abadi, I., Shaham, D., & Grosman, L. (2019). Lime plaster cover of the dead 12,000 years ago – new evidence for the origins of lime plaster technology. *Evolutionary Human Sciences*, *1*. https://doi.org/10.1017/ehs.2019.9

Garfinkel, Y. (1987). Burnt Lime Products and Social Implications in the Pre-Pottery Neolithic B Villages of the Near East. *Paléorient*, *13*(1), 69–76. https://doi.org/10.3406/paleo.1987.4417

Goren, Y., & Goring-Morris, A. N. (2008). Early pyrotechnology in the near east: Experimental lime-plaster production at the pre-pottery neolithic B site of Kfar HaHoresh, Israel. *Geoarchaeology*, *23*(6), 779–798. https://doi.org/10.1002/gea.20241

Goren, Y., & Goldberg, P. (1991). Special Studies: Petrographic Thin Sections and the Development of Neolithic Plaster Production in Northern Israel. *Journal of Field Archaeology*, *18*(1), 131–140.

Gourdin, W. H., & Kingery, W. D. (1975). The Beginnings of Pyrotechnology : Neolithic and Egyptian Lime Plaster. *Journal of Field Archaeology*, *2*(1), 133–150. https://doi.org/10.1179/009346975791491277

Greenhut, Z., De-Groot, A., & Barzilay, E. (2009). *Salvage excavations at Tel Moza : the Bronze and Iron Age settlements and later occupations*. Israel Antiquities Authority.

Grosman, L., Raz, T., & Friesem, D. E. (2020). Tomorrow's mundane is today's extraordinary: A case study of a plastered installation during Neolithization. *Humanities and Social Sciences Communications*, *7*(1), 1–13. https://doi.org/10.1057/s41599-020-00579-8

Hershkovitz, I., Zohar, I., Segal, I., Speirs, M. S., Meirav, O., Sherter, U., Feldman, H., & Goring-Morris, N. (1995). Remedy for an 8500 year-old plastered human skull from Kfar Hahoresh, Israel. *Journal of Archaeological Science*, *22*(6), 779–788. https://doi.org/10.1016/0305-4403(95)90007-1

Jeon, I. K., Kim, H. G., Jakhrani, S. H., & Ryou, J. S. (2021). Evaluation of the microstructure, mechanical, and durability properties of alkali-activated slag-based mortar with light-burnt dolomite powder. *Journal of Materials Research and*

Technology, *13*, 2220–2228. https://doi.org/10.1016/j.jmrt.2021.06.024

Karkanas, P. (2007). Identification of Lime Plaster in Prehistory Using Petrographic Methods: A Review and Reconsideration of the Data on the Basis of Experimental and Case Studies. *Geoarchaeology*, *22*(7), 775–796. https://doi.org/10.1002/gea.20186

Khalaily, H., Milevski, I., Getzov, N., Hershkovitz, I., Barzilai, O., Yarosevich, A., Shlomi, V., Najjar, A., Zidan, O., Smithline, H., & Liran, R. (2008). Recent Excavations at the Neolithic Site of Yiahel (Khalet Khalladyiah), Lower Galilee. *Neo-Lithics*, *2*(March 2016), 3–11.

Khalaily, H., & Vardi, J. (2020). The New Excavations at Motza: An Architectural Perspective on a Neolithic 'Megasite' in the Judean Hills. In Hamoudi Khalaily, A. Re'em, J. Vardi, & I. Milevski (Eds.), *The Mega Project at Motza (Moẓa): The Neolithic and Later Occupations up to the 20th Century* (pp. 69–100). Israel Antiquities Authority. https://doi.org/10.2307/j.ctv1b9f5bh

Khalaily, H., & Vardi, J. (2019). Moza - preliminary report. *Hadashot Arkheologiyot*, *131*.

Kingery, W. D., Vandiver, P. B., & Prickett, M. (1988). The beginnings of pyrotechnology, part ii: Production and use of lime and gypsum plaster in the pre-pottery neolithic near east. *Journal of Field Archaeology*, *15*(2), 219–243. https://doi.org/10.1179/009346988791974501

Lane, M. D. (1999). Midinfrared optical constants of calcite and their relationship to particle size effects in thermal emission spectra of granular calcite. *Journal of Geophysical Research: Planets*, *104*(E6), 14099–14108. https://doi.org/10.1029/1999JE900025

LeChevallier, M. (1978). *Abou Gosh et Beisamoun: Deux Gisements du VIIe Mille´naire avant L'e`re Chretienne en Israel*. Association Paléorient.

Miriello, D., Bloise, A., Crisci, G. M., Apollaro, C., & La Marca, A. (2011). Characterisation of archaeological mortars and plasters from kyme (Turkey). *Journal of Archaeological Science*, *38*(4), 794–804. https://doi.org/10.1016/j.jas.2010.11.002

Newton, R. G., & Sharp, J. H. (1987). An investigation of the chemical constituents of some renaissance plasters. *Studies in Conservation*, *32*(4), 163–175. https://doi.org/10.1179/sic.1987.32.4.163

Poduska, K. M., Regev, L., Berna, F., Mintz, E., Milevski, I., Khalaily, H., Weiner, S., & Boaretto, E. (2012). Plaster characterization at the PPNB site of yiftahel (Israel) including the use of 14C: Implications for plaster production, preservation, and dating. *Radiocarbon*, *54*(3–4), 887–896. https://doi.org/10.1017/S0033822200047536

Poduska, K. M., Regev, L., Boaretto, E., Addadi, L., Weiner, S., Kronik, L., & Curtarolo, S. (2011). Decoupling local disorder and optical effects in infrared spectra: Differentiating between calcites with different origins. *Advanced Materials*, *23*(4), 550–554. https://doi.org/10.1002/adma.201003890

Querry, M. (1987). *Optical Constants of Minerals and Other Materials from the Millimeter to the Ultraviolet*.

Regev, L., Poduska, K. M., Addadi, L., Weiner, S., & Boaretto, E. (2010). Distinguishing between calcites formed by different mechanisms using infrared spectrometry: Archaeological applications. *Journal of Archaeological Science*, *37*(12), 3022–3029. https://doi.org/10.1016/j.jas.2010.06.027

Regev, L., Zukerman, A., Hitchcock, L., Maeir, A. M., Weiner, S., & Boaretto, E. (2010). Iron Age hydraulic plaster from Tell es-Safi/Gath, Israel. *Journal of Archaeological Science*, *37*(12), 3000–3009. https://doi.org/10.1016/j.jas.2010.06.023

Rollefson, G. O. (1990). The uses of plaster at Neolithic Ain Ghazal, Jordan. *Archaeomaterials*, *4*(1), 33–54.

Roskin, J., Asscher, Y., Khalaily, H., Ackermann, O., & Vardi, J. (2022). The palaeoenvironment and the environmental impact of the Pre - Pottery Neolithic Motza megasite and its surrounding Mediterranean landscape in the central Judean Highlands (Israel). *Mediterranean Geoscience Reviews*, *0123456789*. https://doi.org/10.1007/s42990-022-00076-x

Ryb, U., & Eiler, J. M. (2018). Oxygen isotope composition of the Phanerozoic ocean and a possible solution to the dolomite problem. *Proceedings of the National Academy of Sciences of the United States of America*, *115*(26), 6602–6607. https://doi.org/10.1073/pnas.1719681115

Scannell, S., Lawrence, M., & Walker, P. (2014). Impact of aggregate type on air lime mortar properties. *Energy Procedia*, *62*, 81–90. https://doi.org/10.1016/j.egypro.2014.12.369

Schirmer, W. (1990). Some aspects of building at the 'aceramic-neolithic' settlement of Çayönü Tepesi. *World Archaeology*, *21*(3), 363–387. https://doi.org/10.1080/00438243.1990.9980114

Štukovnik, P., Bokan Bosiljkov, V., & Marinšek, M. (2020). Alkali-dolomite reaction in air lime mortar – implications for increased strength and water resistance. *Journal of Cultural Heritage*, *45*, 160–168. https://doi.org/10.1016/j.culher.2020.02.007

Thuesen, I., Leonardsen, E., Rehhoff, L., & Akkermans, P. M. M. G. (1990). Plasters: Gypsum or Calcite? A Preliminary Case Study of Syrian Plasters. *Paléorient*, *16*, 79–87. https://doi.org/10.3406/paleo.1990.4534

Toffolo, M. B., Regev, L., Dubernet, S., Lefrais, Y., & Boaretto, E. (2019). FTIR-Based crystallinity assessment of aragonite-calcite mixtures in archaeological lime binders altered by diagenesis. *Minerals*, *9*(2). https://doi.org/10.3390/min9020121

Toffolo, M. B., Regev, L., Mintz, E., Kaplan-Ashiri, I., Berna, F., Dubernet, S., Yan, X., Regev, J., & Boaretto, E. (2020). Structural Characterization and Thermal Decomposition of Lime Binders Allow Accurate Radiocarbon Age Determinations of Aerial Lime Plaster. *Radiocarbon*, *62*(3), 633–655. https://doi.org/10.1017/RDC.2020.39

Vardi, J., & Khalaily, H. (2021). Moza, Section A. *Hadashot Arkheologiyot*, *133*.

Warren, J. (2000). Dolomite: Occurence, evolution and economically important associations. *Earth Science Reviews*, *52*(1–3), 1–81. https://doi.org/10.1016/S0012-8252(00)00022-2

Xu, B., & Poduska, K. M. (2014). Linking crystal structure with temperature-sensitive vibrational modes in calcium carbonate minerals. *Physical Chemistry Chemical Physics*, *16*(33), 17634–17639. https://doi.org/10.1039/c4cp01772b

Xu, B., Toffolo, M. B., Boaretto, E., & Poduska, K. M. (2016). Assessing Local and Long-Range Structural Disorder in Aggregate-Free Lime Binders. *Industrial and Engineering Chemistry Research*, *55*(30), 8334–8340. https://doi.org/10.1021/acs.iecr.6b01785

Xu, B., Toffolo, M. B., Regev, L., Boaretto, E., & Poduska, K. M. (2015). Structural differences in archaeologically relevant calcite. *Analytical Methods*, *7*(21), 9304–9309. https://doi.org/10.1039/c5ay01942g

Zhang, X., Luo, Y., & Yao, W. (2021). Influences of the dosage of dolomite powder on the fracture properties and volume stability of cement-based materials. *Fullerenes Nanotubes and Carbon Nanostructures*, *29*(11), 868–875. https://doi.org/10.1080/1536383X.2021.1900125

Supplementary Information

Table SI-1: Calcite spar and dolomite (Motza bedrock) FTIR calibration data

sample	calcite spar (mg)	dolomite Motza bedrock (mg)	% dolomite (w/w)	average FTIR 728/(713+728) (n=9)	stdv
1	44.6	5.0	10.1	0.128	0.021
2	28.7	9.3	24.5	0.277	0.054
3	19.2	19.1	49.9	0.452	0.024
4	9.8	31.1	76.0	0.631	0.059
5	5.4	46.4	89.6	0.787	0.031

Table SI-2: The FTIR data of the different building phases in area B10 case study, showing the normalized peak heights of calcite ν_2 and ν_4, the ratio of silicates to carbonates (Si/CO3), the ratio of the dolomite and calcite ν_4 peaks, 728/(713+728), and the % dolomite of carbonates calculated from that ratio.

building phase	layer	locus	basket	ν_2	ν_4	Si/CO_3	$\frac{728}{(713+728)}$	% dolomite (by spar calibration)
1	prep	4666	136135	495	192	0.29	0.51	57.18
1	prep	4666	136135	459	115	0.22	0.65	74.27
1	prep	4666	136132	489	212	0.27	0.32	32.62
1	prep	4666	135550	438	102	0.22	0.57	64.77
1	prep	4666	136322	488	188	0.21	0.45	49.71
1	prep	4666	136322	394	101	0.08	0.35	36.80
1	prep	4666	136323	476	160	0.23	0.31	31.23
1	prep	4666	136330	452	112	0.19	0.45	49.33
1	prep	4666	136330	418	100	0.14	0.44	48.44
1	prep	4666	136129	461	148	0.41	0.36	38.32
1	prep	4721	136134	575	158	0.20	0.27	26.29
1	prep	4721	136331	453	112	0.15	0.42	44.90
1	prep	4681	136136	488	167	0.21	0.40	43.00
1	prep	4681	136321	502	185	0.24	0.46	49.84
1	topcoat	4666	136322	510*	143	0.11	0.08	2.87
1	topcoat	4666	136322	540*	173	0.12	0.08	2.11
1	topcoat	4666	136135	465	94	0.07	0.19	16.04
1	topcoat	4666	136135	445	94	0.17	0.32	32.75
1	topcoat	4666	136135	445	96	0.09	0.16	12.11
1	topcoat	4666	136429	377	66	0.06	0.15	10.85
1	topcoat	4666	136428	452	90	0.07	0.14	9.96
1	topcoat	4681	136136	294	46	0.14	0.49	54.01
1	topcoat	4681	136321	449	107	0.26	0.41	43.89
2	prep	4622	135740	431	147	0.25	0.25	23.63
2	prep	4622	plaster8	450	124	0.39	0.60	67.56
2	prep	4622	136130	409	150	0.37	0.16	12.87

building phase	layer	locus	basket	ν_2	ν_4	Si/CO_3	$\frac{728}{(713+728)}$	% dolomite (by spar calibration)
2	prep	4622	136329	400	85	0.36	0.36	37.94
2	prep	4716	136124	353	65	0.14	0.49	54.39
2	prep	4716	136124	363	77	0.17	0.48	52.37
2	prep	4622	136126	421	135	0.34	0.35	36.80
2	prep	4622	136326	496	186	0.26	0.32	33.13
2	prep	4622	136125	456	163	0.24	0.52	58.06
2	prep	4622	136125	534	168	0.38	0.62	70.22
2	prep	4622	136325	429	133	0.17	0.35	36.04
2	prep	4622	136332	512	138	0.32	0.57	64.52
2	prep	4622	136131	473	140	0.21	0.43	46.80
2	prep	4716	136127	336	67	0.19	0.37	38.82
2	topcoat	4622	136329	476	116	0.18	0.15	11.73
2	topcoat	4716	136124	414	101	0.08	0.07	1.10
2	topcoat	4716	136124	366	71	0.04	0.07	0.97
2	topcoat	4622	136426	410	76	0.07	0.12	7.94
2	topcoat	4622	136326	499	117	0.08	0.08	2.87
2	topcoat	4622	136332	518	128	0.07	0.12	6.80
2	topcoat	4622	136427	439	87	0.07	0.11	6.67
2	topcoat	4716	136127	464	106	0.07	0.08	2.87
2/3	topcoat	4642	136122	374	65	0.05	0.10	4.77
2/3	prep	4642	136122	404	94	0.19	0.43	47.05
1	prep - light**	4666	136322	413	83	0.12	0.14	10.22
1	prep - light	4666	136330	358	60	0.40	0.26	25.03
2	prep - light	4622	136126	411	88	0.29	0.14	9.71
2	prep - light	4622	136329	379	72	0.29	0.13	8.32

*Sample contains a small amount of aragonite

**Light = The light fraction after density separation in SPT.